Journal of Power Sources 195 (2010) 419–424

Contents lists available at ScienceDirect

Journal of Power Sources

journal homepage: www.elsevier.com/locate/jpowsour

Controlling the morphology and uniformity of a catalyst-infiltrated cathode for solid oxide fuel cells by tuning wetting property

Xiaoyuan Lou[a], Ze Liu[a], Shizhong Wang[a], Yonghao Xiu[a,b], C.P. Wong[a], Meilin Liu[a,*]

[a] School of Materials Science and Engineering, Georgia Institute of Technology, Atlanta, GA 30332-0245, USA
[b] School of Chemical and Biomolecular Engineering, Georgia Institute of Technology, Atlanta, GA 30332-0100, USA

ARTICLE INFO

Article history:
Received 9 July 2009
Accepted 28 July 2009
Available online 5 August 2009

Keywords:
Solid oxide fuel cell
LSCF
SSC
Cathode modification
Infiltration
Wetting

ABSTRACT

Infiltration has been widely used in surface modification of porous electrodes in solid oxide fuel cells (SOFCs). The stability and performance of a porous electrode infiltrated with a catalyst depend sensitively on the composition, morphology, and nanostructure of the catalyst. In this contribution, we report our findings on investigation into the effect of wetting property on the formation of catalyst coatings through an infiltration process. It is observed that aqueous solutions containing catalyst precursors wet SOFC electrolyte materials (e.g., yttria-stabilized zirconia or YSZ) better than cathode materials (e.g., $La_{0.6}Sr_{0.4}Co_{0.2}Fe_{0.8}O_{3-\delta}$ or LSCF). Controlling the wetting of catalyst precursor solutions on porous electrode backbones can dramatically improve the uniformity of the infiltrated catalyst layer on porous cathode backbone, thus enhancing the electrochemical performance of infiltrated cathodes, especially at low operating temperatures.

1. Introduction

Solution infiltration (or impregnation) has recently attracted more interests for its application in solid oxide fuel cells (SOFCs) to introduce a catalytically active layer on the surface of a porous electrode [1–10]. The larger surface area and heterogeneous microstructure created by infiltration can dramatically enhance not only the ionic and electronic conductivity but also the surface catalytic behavior. It is expected that surface modification with a proper catalyst has a potential to increase both performance and stability of the state-of-the-art SOFC electrodes.

To achieve a better cell performance, the developments of active catalysts with desired microstructures are critical [5]. To retain such enhancement, a stable and uniformly distributed coating inside a well-sintered backbone is necessary. An infiltration process involves the precipitation and decomposition of a metal salt solution inside a porous electrode or electrolyte structure. Ideally, the infiltrated catalyst material should form a thin and continuous network on the grain surface of the backbone in order to enhance both surface catalytic property and electronic/ionic conductivity [5]. Furthermore, such internal coating should not impede gas transport within the pores of the electrode. Thus, engineering these surface catalyst networks inside the porous electrode is necessary for optimizing the performance.

Multiple-step impregnation has been demonstrated by Jiang [1] as an effective way to continuously improve electrode structure for better performance. Later, it has also been demonstrated that similar performance enhancement can be accomplished using a one-step infiltration process with the assistance of surfactant [4,5], providing an easy and efficient way for surface modification. More importantly, it avoids any degradation, failure and defects during the multiple infiltration and calcination steps. However, the challenge for a successful one-step infiltration process is how to best optimize various processing parameters in order to achieve the desired nanostructure in one single step [5].

Strontium- and iron-doped lanthanum cobaltites, $La_xSr_{1-x}Co_yFe_{1-y}O_{3-\delta}$, have been considered as a good cathode material for intermediate temperature application [11–13]. Infiltration has been used to further improve its performance [5,10,14]. Due to the performance degradation of LSCF at high temperature [15], one-step infiltration process is extremely important to avoid any possible degradation associated with multiple-step calcination procedures. Currently, infiltration is mostly applied to porous electrolyte backbones such as YSZ because a porous electrolyte skeleton fired at high temperatures usually provides excellent mechanical integrity [4,16–18]. In contrast, infiltration of catalysts into a porous cathode backbone is still a challenge because it is mechanically much weaker than the porous electrolyte backbone.

In this study, we investigated how surface wetting property influenced the formation of $Sm_{0.6}Sr_{0.4}CoO_{3-\delta}$ (SSC) nanostructured coatings inside a porous LSCF cathode during an infiltration pro-

* Corresponding author. Tel.: +1 404 894 6114; fax: +1 404 894 9140.
E-mail address: meilin.liu@mse.gatech.edu (M. Liu).

0378-7753/$ – see front matter © 2009 Elsevier B.V. All rights reserved.
doi:10.1016/j.jpowsour.2009.07.048

cess. Since aqueous solution of SSC does not wet LSCF, it is vital to modify the surface tension of the precursor solution in order to control the morphology and microstructure of SSC, and thus enhance the electrochemical performance of SSC infiltrated LSCF cathodes.

2. Experimental

2.1. Fabrication of symmetric cells

$Gd_{0.1}Ce_{0.9}O_{1.95}$ (GDC) was used as the electrolyte due to its high ionic conductivity at intermediate temperatures and good compatibility with LSCF. Symmetric cells with the configuration of LSCF |GDC| LSCF were fabricated as follows: GDC pellets were pressed uniaxially and sintered at 1450 °C for 5 h to ensure relative density of 98%. LSCF powder was prepared using a citrate method [19] fired at 850 °C for 2 h, resulting in an average particle size of 20–50 nm and a surface area of 13.62 $m^2\,g^{-1}$. Under a mixing ratio (wt.%) of 2:1:1 using LSCF powder, binder (Heraeus V-006) and solvent (acetone), LSCF slurry was made by ball-milling for 2 h. Then LSCF slurry was screen-printed on both sides of the GDC pellet to form LSCF |GDC| LSCF symmetric cell. After firing at 1080 °C for 2 h, porous LSCF electrode was obtained with the thickness around 30 μm. Shown in Fig. 1 is the SEM image of blank porous LSCF cathode after sintering. The average grain size was around 200 nm.

2.2. Infiltration

1.44 mol L^{-1} SSC precursor solution was prepared by mixing $Sm(NO_3)_3{\cdot}6H_2O$, $Sr(NO_3)_2$, $Co(NO_3)_2{\cdot}6H_2O$ and surfactant in water with corresponding molar ratios. Various surfactants were tested and urea was selected as the best complex agent to form a correct perovskite phase. Ethanol was added into the aqueous solution with different ratios to modify the liquid surface tension on LSCF backbone. A micro-liter syringe was applied to infiltrate 7 μL of solution into each cathode side for precise control. Vacuum apparatus helped to force the liquid into micropores. The infiltrated cell was then calcined at 800 °C for 1 h.

2.3. Electrochemical testing

The symmetric cell was sandwiched between two 100 mesh Pt grids as the working and counter electrodes for testing. Solartron 1287 potentiostat and 1860 frequency analyzer were used to perform the electrochemical impedance analysis. Both sides of symmetric cell were exposed to uniform oxygen atmosphere. One Pt wire was attached to one side as a reference electrode. Under open circuit voltage (OCV), 10 mV AC signal in a frequency range of 0.1 Hz to 1 MHz was applied to obtain the impedance spectra.

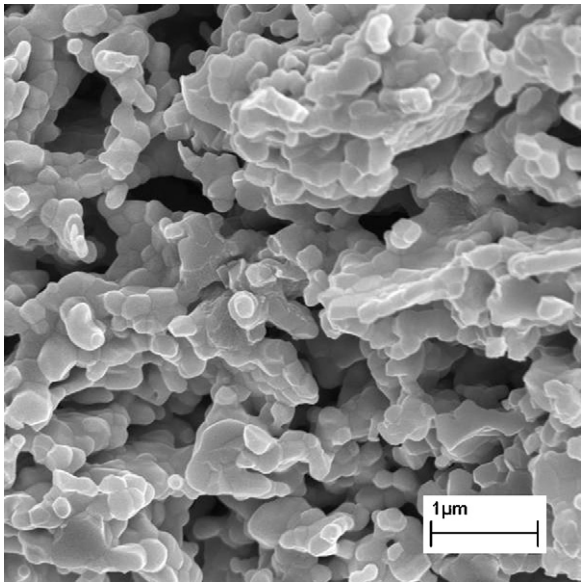

Fig. 1. Microstructure of a blank porous LSCF cathode after sintering.

2.4. Contact angle measurement

In order to study the surface wetting properties, dense pellets of LSCF, LSM, YSZ and GDC were uniaxially pressed and fired at 1350 °C or higher for 5 h. The samples were all polished to <1 μm surface roughness to obtain flat and smooth surfaces for contact angle measurement. Wetting contact angle was measured using a Rame-Hart contact angle goniometer.

2.5. Physical characterization

Phase identification was conducted on an X'Pert PRO Alpha-1 X-ray diffractometer using Cu Kα radiation. Microstructure characterization was carried out using a LEO 1530 thermally assisted field emission scanning electron microscope.

3. Results and discussion

It has been noted that the choice of surfactant plays an important role in the nanostructured cathode fabrication, including one-step infiltration process [5,20,21]. Surfactant not only complexes with metal cations to assist the formation of crystalline phase, but also controls the particle size through a proper micelle formation. Shown in Fig. 2(a) are the X-ray diffraction (XRD) patterns of SSC powders derived from solutions with different surfactants. The molar ratios of metal cations to surfactants used in this study were all overloaded to ensure enough complexing agents were present in the precursor. The detailed molar ratios are shown in Fig. 2(a). All infiltrated samples were fired at 800 °C for 1 h followed by XRD to determine the phase composition. Both urea and citric acid could assist SSC precursor to form the desired perovskite phase. In the absence of a proper surfactant, however, second phases were also identified. Previous work showed that Triton X series surfactants were perfect for LSM phase formation [4,5]. For SSC, however, both Triton X-45 and X-100 did not yield a pure perovskite phase firing under the same conditions. Because the acidity of citric acid could potentially attack weakly bonded oxide structure of cathode, urea was chosen in this work as a surfactant for SSC infiltration. Fig. 2(b) shows the SSC phase formation under different urea loadings. The XRD patterns indicated a perfect perovskite phase could be achieved when the molar ratios of urea to SSC were greater than 10:1.

Wetting contact angles of precursor solutions with different water-to-ethanol volume ratios were measured on flat and dense LSCF, LSM, YSZ, and GDC substrates. These materials are the most common backbone candidates for SOFCs infiltration. As shown in Fig. 3, the aqueous solution of SSC exhibited higher contact angles on LSCF and LSM substrates than YSZ and GDC substrates, due mainly to higher surface tension. Ethanol usually has a lower surface tension than water. At room temperature, for example, the surface tension of ethanol against air is around 22 dynes cm^{-1}, while that of water is around 72 dynes cm^{-1} [22]. Therefore, by adding ethanol into water, the intermolecular solvation can dramatically improve the surface wetting property. Fig. 3 shows the decreases of contact angles as the ratios of ethanol-to-water were increased in the precursor solutions. When the water-to-ethanol ratio reached 1:0.6, the precursor solution displayed similar low contact angles on all substrates.

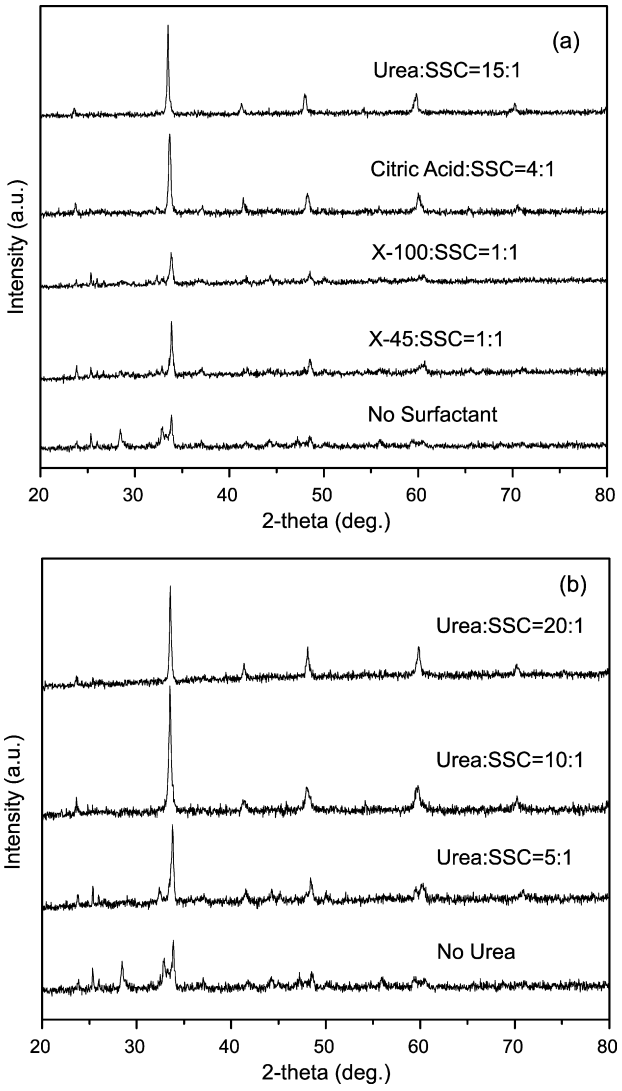

Fig. 2. Typical X-ray diffraction patterns of SSC derived from the precursor solutions for SSC infiltration showing the effects on phase formation of (a) surfactants used and (b) the loading amounts of urea.

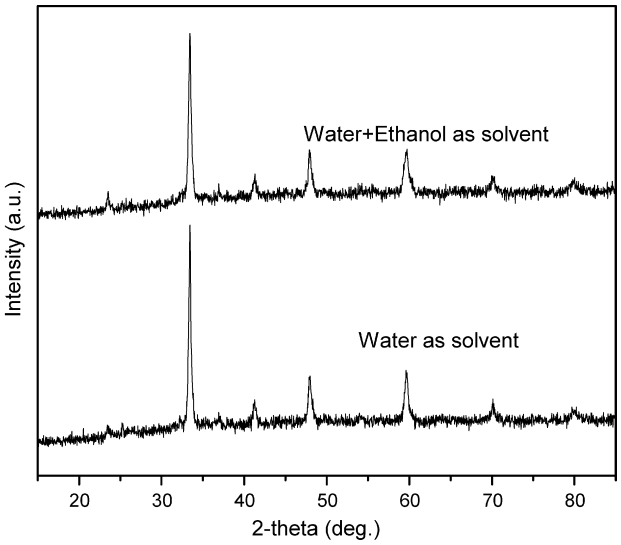

Fig. 4. X-ray diffraction patterns of the SSC derived from SSC precursor solutions using different solvents: (a) water and (b) water + ethanol.

Shown in Fig. 4 are some typical X-ray diffraction patterns of the samples derived from solutions with and without addition of ethanol. Both samples exhibited pure SSC perovskite phase. Since ethanol and water are completely miscible and urea can dissolve in both water and ethanol, metal cations can be easily solvated and complexed through ethanol and water molecules due to intermolecular interaction. Thus, the addition of ethanol did not influence the metal cation complexation and the formation of the single phase SSC through infiltration.

Shown in Fig. 5 indicates how the surface wetting affects the morphology of a derived coating on a flat substrate. 2 μL of SSC precursor solutions with and without ethanol were dropped on two identical flat LSCF dense substrates. Two samples went through the same post-firing process. In Fig. 5(a), SSC coating grew uniformly on the LSCF substrate by using a precursor solution containing ethanol. The coating was continuous except for some visible cracks, due probably to the mismatch in thermal expansion coefficient of a thick film. In contrast, as shown in Fig. 5(b), the coating derived from an aqueous precursor solution without ethanol showed agglom-

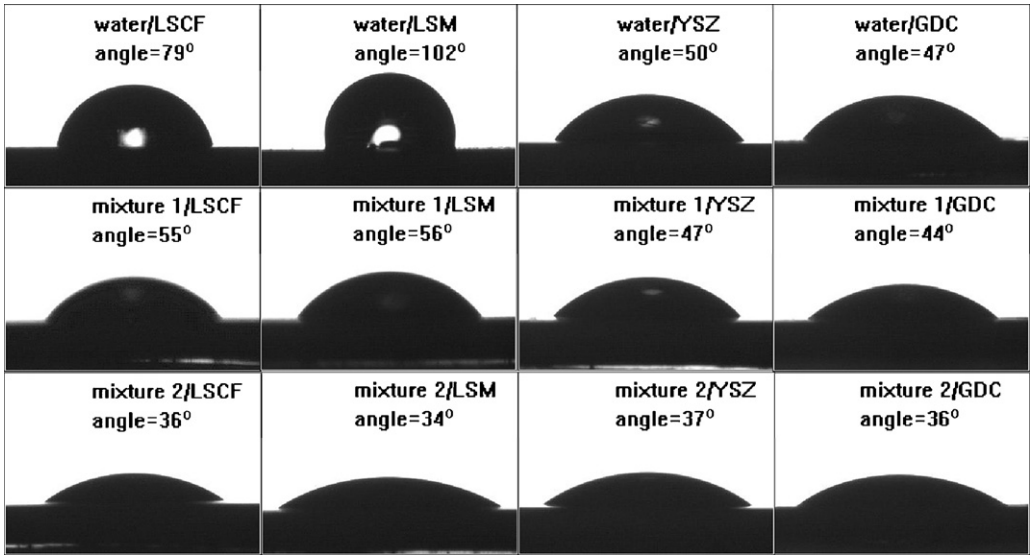

Fig. 3. Wetting angles of different SSC precursor solutions on LSCF, LSM, YSZ and GDC substrates (*note*: mixture 1 had a water-to-ethanol volume ratio of 1:0.3 and mixture 2 has a water-to-ethanol volume ratio of 1:0.6).

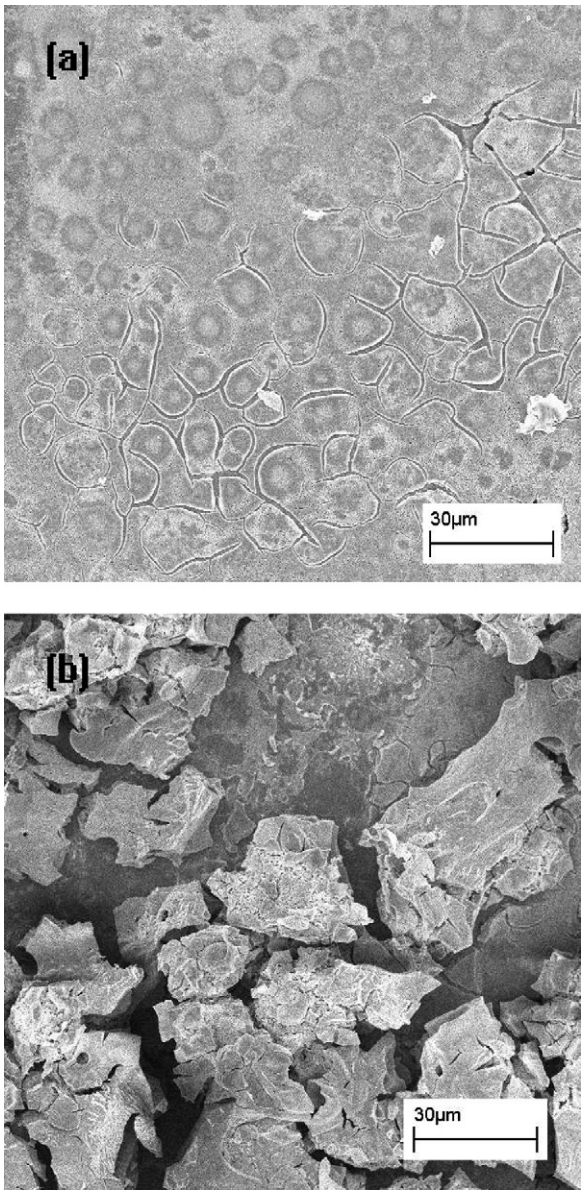

Fig. 5. Typical morphologies of SSC coatings on a dense LSCF substrate prepared by a drop coating process (dropping 2 μL SSC precursor solution on a polished dense LSCF substrate followed by firing at 800 °C for 1 h): (a) 1.44 M SSC nitrate solution with water:ethanol = 1:0.6; (b) 1.44 M SSC nitrate aqueous solution (without ethanol).

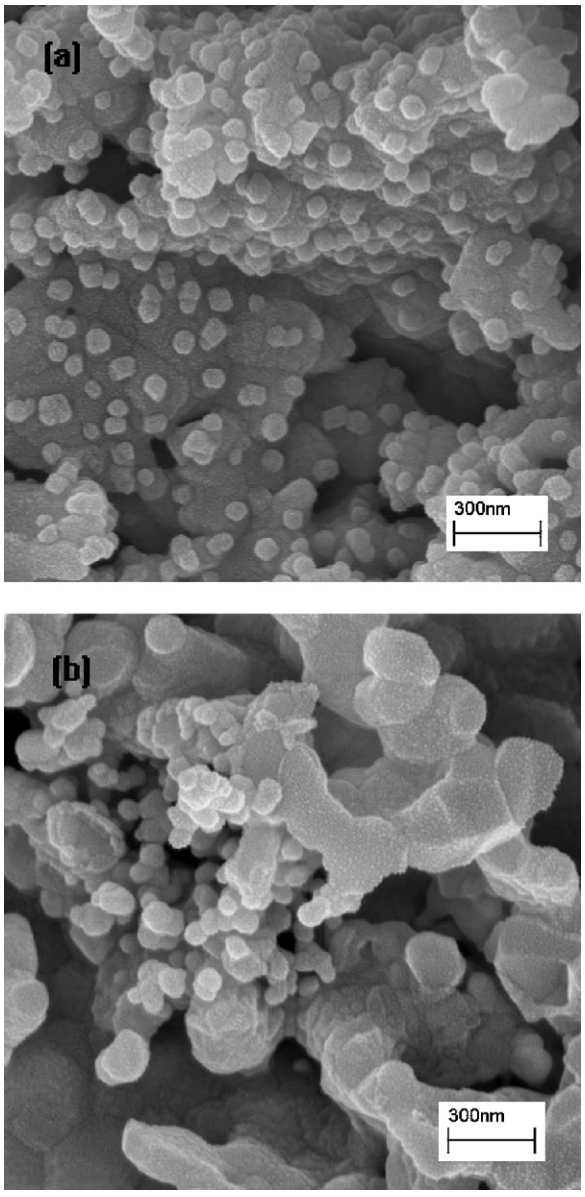

Fig. 6. Typical morphologies of SSC nanoparticles infiltrated into porous LSCF cathode backbone: (a) 1.44 M SSC nitrate solution with water:ethanol = 1:0.6; (b) 1.44 M SSC nitrate aqueous solution (without ethanol).

erated particulate islands on a flat LSCF substrate. A poor surface wetting property created liquid beads or islands standing on the substrate. In the post-firing process, the strong surface tension tended to hold these liquid beads and form agglomerated particulate clusters. Therefore, in order to achieve a uniform coating on the surface, controlling the wetting property of the precursor solution is important.

Similar agglomeration of SSC nanoparticles could also take place inside the porous LSCF cathode backbone after infiltration. Shown in Fig. 6 are some typical cross-sectional views of LSCF porous cathodes infiltrated with SSC solutions. For the sample infiltrated with 1.44 mol L^{-1} SSC solution using a mixed solvent of water and ethanol, a well-distributed SSC layer was observed on the surface of porous LSCF backbone, as shown in Fig. 6(a). SSC nanoparticles (of 40–80 nm in diameter) uniformly spread on LSCF grain surface. In contrast, for the sample infiltrated with SSC solutions without ethanol, SSC nanoparticles tended to agglomerate together, leaving other grains without surface modification, as shown in Fig. 6(b). Because of the poor wetting property between water and LSCF, initial nucleation of SSC phase was localized in small liquid beads which had poor intermolecular bonding to the backbone grain. Such SSC phase grew in the form of nanoparticulate cluster instead of thin coating on the grain surface, resulting in a non-uniform catalyst coverage inside the porous backbone.

The morphologies of the catalyst coatings greatly influence the electrochemical performances of the infiltrated cathodes. Fig. 7 shows some typical electrochemical impedance spectra of the infiltrated cathodes with and without the addition of ethanol in precursor solutions. The amounts of precursor loading were the same (7 μL, 1.44 mol L^{-1}) for both cells. The spectra were collected about 1 h after the cells reached the steady state condition. The differences in bulk resistances of these cells were within 5%, indicating that all the symmetric cells were similar, as they were fabricated under the same conditions. In order to compare the polarization resistance clearly, all bulk resistances were removed from the spectra. At 750 °C, both cells exhibited similar interfacial resistances of

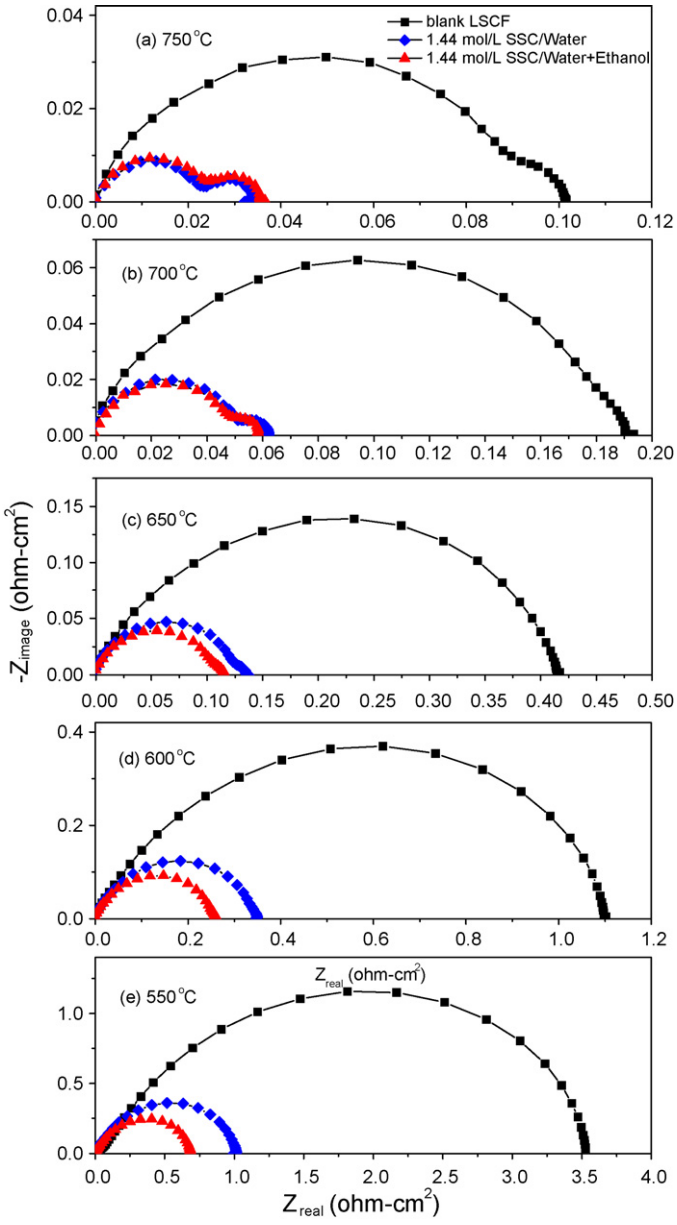

Fig. 7. Impedance spectra of LSCF cathodes with different infiltration treatments as measured in air under open circuit conditions at different temperatures: (a) 750 °C; (b) 700 °C; (c) 650 °C; (d) 600 °C; (e) 550 °C.

$\sim$0.036 $\Omega\,cm^{-2}$. It appeared that the difference in SSC coating structure, as revealed in Fig. 6, had little influence on cell performance at high temperatures. As the operating temperature was reduced, however, the precursor wetting property began to influence the cathode performance. The cathode infiltrated with the aqueous precursor solution (without ethanol) exhibited higher interfacial resistance, more so at lower operating temperatures. At 550 °C, for instance, the interfacial resistances were 0.69 and 1.0 $\Omega\,cm^{-2}$, respectively for the case with and without the addition of ethanol. Although they both were much lower than the resistance of a blank LSCF cell (3.52 $\Omega\,cm^{-2}$), the addition of ethanol improved the dispersion of SSC coating on LSCF, thus enhancing the performance by 30%. Uniformly distributed SSC nanoparticles yielded a higher performance enhancement on LSCF backbone, especially at lower temperatures.

Schematically illustrated in Fig. 8 are the representative microstructures and morphologies for SSC infiltrated LSCF cathodes. Uniformly distributed SSC coating provided a uniform particulate layer on LSCF grains, as shown in Fig. 8(a). Such a catalyst layer (<100 nm thick) facilitated the reduction of oxygen on the cathode surface and thus reduced the interfacial polarization resistance of an SSC infiltrated LSCF backbone. However, the agglomerated SSC particles resulted in bulky clusters, as shown

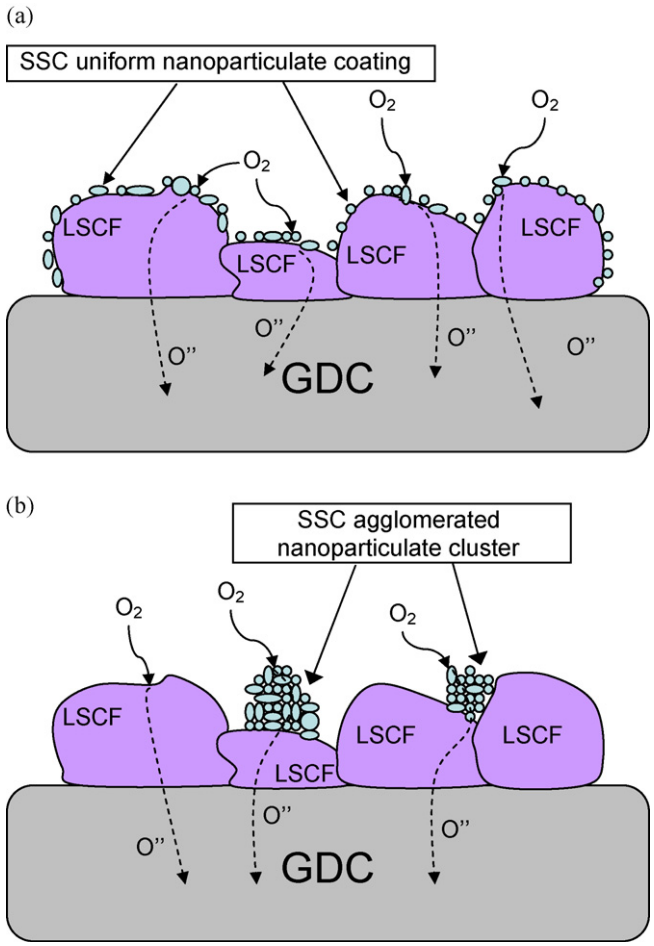

Fig. 8. Schematic illustration of SSC infiltrated LSCF cathodes: (a) uniformly distributed nanoparticulate coating in porous backbone; (b) agglomerated nanoparticles in porous backbone.

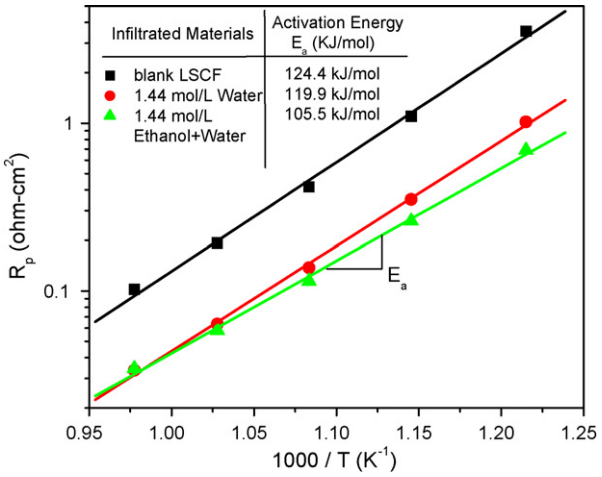

Fig. 9. Interfacial resistances and activation energies of blank and SSC infiltrated LSCF cathodes, as determined from impedance spectra collected under open circuit conditions.

in Fig. 8(b), which might not be effective in reducing the interfacial polarization resistance, especially at low temperatures. While the performances of the SSC infiltrated LSCF cathodes with different morphologies were similar at 750 °C, the cathodes with a uniform SSC thin layer showed much better performance at lower temperatures than the ones with non-uniform SSC coatings. The bulky SSC cluster provided less active reaction zone for oxygen reduction compared with the uniform SSC surface layer.

Fig. 9 compares the interfacial polarization resistances of blank and SSC infiltrated LSCF cathodes using two types of precursors. Both SSC infiltrated LSCF cathodes exhibited lower activation energy than blank LSCF cathode. The cathode infiltrated with a uniform SSC coating showed a much lower activation energy ($105.5\,kJ\,mol^{-1}$) than the one with a less uniform coating of SSC ($119.9\,kJ\,mol^{-1}$), suggesting that the distribution and morphology of the SSC surface layer played an important role in reducing reaction barrier. By controlling the wetting property of the precursor solution, we are able to improve the uniformity of SSC nanoparticulate coating in order to further improve LSCF cathode activity, especially at low operating temperatures.

4. Conclusions

We have demonstrated that the infiltration of LSCF backbone with an SSC solution can considerably improve the performance of LSCF cathodes. However, the performance of an SSC infiltrated LSCF depended sensitively on the microstructure and morphology of the SSC coatings, which in term, depended on the wetting property of the SSC precursor solutions. Ethanol was proven to be an effective additive to the SSC nitrate precursor solution to lower its surface tension on LSCF backbone, leading to uniform and continuous SSC coatings on LSCF and superior cell performance at low temperatures. This work provided a promising way to further engineer the one-step infiltration method for modifying low-temperature cathodes in existing SOFCs.

Acknowledgements

This work was supported by the DOE-NETL SECA Core Technology Program under Grant Number DE-NT0006557. The authors gratefully acknowledge valuable discussions with DOE project manager Dr. Briggs White.

References

[1] S.P. Jiang, Mater. Sci. Eng. A 418 (1–2) (2006) 199.
[2] S.P. Jiang, S. Zhang, Y.D. Zhen, A.P. Koh, Electrochem. Solid-State Lett. 7 (9) (2004) A282.
[3] S.D. Park, J.M. Vohs, R.J. Gorte, Nature 404 (6775) (2000) 265.
[4] T.Z. Sholklapper, C. Lu, C.P. Jacobson, S.J. Visco, L.C. De Jonghe, Electrochem. Solid-State Lett. 9 (8) (2006) A376.
[5] T.Z. Sholklapper, H. Kurokawa, C.P. Jacobson, S.J. Visco, L.C. De Jonghe, Nano Lett. 7 (7) (2007) 2136.
[6] A. Atkinson, S. Barnett, R.J. Gorte, J.T.S. Irvine, A.J. McEvoy, M. Mogensen, S.C. Singhal, J. Vohs, Nat. Mater. 3 (1) (2004) 17.
[7] M. Shah, J.D. Nicholas, S.A. Barnett, Electrochem. Commun. 11 (1) (2009) 2.
[8] Q. Zhang, B.E. Martin, A. Petric, J. Mater. Chem. 18 (36) (2008) 4341.
[9] T.Z. Sholklapper, V. Radmilovic, C.P. Jacobson, S.J. Visco, L.C. De Jonghe, J. Power Sources 175 (1) (2008) 206.
[10] X.Y. Lou, S.Z. Wang, Z. Liu, L. Yang, M.L. Liu, Solid State Ionics, in press (2009), doi:10.1016/j.ssi.2009.06.014.
[11] S.P. Jiang, Solid State Ionics 146 (1–2) (2002) 1.
[12] M.L. Liu, J. Electrochem. Soc. 145 (1) (1998) 142.
[13] J. Fleig, J. Power Sources 105 (2) (2002) 228.
[14] Y. Sakito, A. Hirano, N. Imanishi, Y. Takeda, O. Yamamoto, Y. Liu, J. Power Sources 182 (2) (2008) 476.
[15] S.P. Simner, M.D. Anderson, M.H. Engelhard, J.W. Stevenson, Electrochem. Solid-State Lett. 9 (10) (2006) A478.
[16] T.J. Armstrong, J.G. Rich, J. Electrochem. Soc. 153 (3) (2006) A515.
[17] T.Z. Sholklapper, V. Radmilovic, C.P. Jacobson, S.J. Visco, L.C. De Jonghe, Electrochem. Solid-State Lett. 10 (4) (2007) B74.
[18] W.S. Wang, M.D. Gross, J.M. Vohs, R.J. Gorte, J. Electrochem. Soc. 154 (5) (2007) B439.
[19] Z. Liu, M.F. Han, W.T. Miao, J. Power Sources 173 (2007) 837.
[20] M. Mamak, G.S. Metraux, S. Petrov, N. Coombs, G.A. Ozin, M.A. Green, J. Am. Chem. Soc. 125 (17) (2003) 5161.
[21] J.M. Serra, S. Uhlenbruck, W.A. Meulenberg, H.P. Buchkremer, D. Stover, Top. Catal. 40 (1–4) (2006) 123.
[22] J.A. Dean, Lange's Handbook of Chemistry, 15th edition, McGraw-Hill Professional, 1998.